https://doi.org/10.1016/j.conbuildmat.2020.119430

Shear behavior of reinforced concrete beams with GFRP needles

X.F. Nie[1, 2], B. Fu[2, 3, *], J.G. Teng[2], L.C. Bank[4] and Y. Tian[5]

[1] School of Civil Engineering and Mechanics, Huazhong University of Science and Technology, Wuhan 430074, China.
[2] Department of Civil and Environmental Engineering, The Hong Kong Polytechnic University, Hong Kong, China.
[3] School of Civil and Transportation Engineering, Guangdong University of Technology, Guangzhou 510643, China.
[4] School of Architecture, Georgia Institute of Technology, Atlanta, GA 30221, USA.
[5] Civil Engineering Department, City College of New York, New York, NY 10031, USA.

Abstract: Fiber-reinforced polymer (FRP) waste is becoming an environmental concern due to the widespread use and non-biodegradable nature of FRP composites. Cutting FRP waste into short-length randomly distributed reinforcing bars (referred to as "needles" hereafter) as a substitute for part of the coarse aggregate in concrete has been suggested as a possible solution to FRP waste recycling. This paper presents to the authors' best knowledge the first reported experimental investigation into the effect of GFRP needles as coarse aggregate partial replacement in concrete on the shear behavior of large-scale reinforced concrete (RC) beams. A total of 10 RC beams without steel stirrups in the critical half were tested under four-point bending. The volume replacement ratio of coarse aggregate and the surface type of GFRP needles were chosen as the test parameters. All test beams failed in shear in a brittle manner with their ductility being slightly enhanced by the partial replacement of coarse aggregate using GFRP needles. An enhancement of 8%-10% in the load-carrying capacity was observed in beams with helically wrapped needles, while beams with smooth needles showed a slight reduction in the load-carrying capacity. The presence of GFRP needles increased the amount of total energy absorbed by the RC beams by about 33%-40%.

Keywords: reinforced concrete (RC) beam; shear behavior; fiber-reinforced polymer (FRP) needle; FRP waste; FRP recycling

[*] Corresponding author. Email: cefubing@gdut.edu.cn

1. INTRODUCTION

Fiber-reinforced polymer (FRP) composites have been extensively and increasingly used in various industries, such as aerospace, marine and construction, for over half a century. An increasing number of FRP vessels, wind turbines and structural components are approaching the end of their service or functional lives, leading to an increasing rate of FRP waste accumulation [1]. Due to the widespread use and non-biodegradable nature of FRP composites, FRP waste is becoming an environmental concern. A variety of methods have been proposed for the recycling of FRP waste [2], and a number of researchers have studied the feasibility of grinding FRP waste into powder as filler of concrete [1,3]. However, grinding FRP waste into powder as filler of concrete consumes a significant amount energy, and may lead to a reduction in the mechanical properties of concrete [2]. Therefore, a more economical and environmentally-friendly approach to recycle FRP waste is desirable. Cutting FRP waste into short-length randomly distributed reinforcing bars of relatively small cross-section (referred to as "needles" hereafter) as a substitute for coarse aggregate in concrete may be a possible solution to address this issue [4-7]. Yazdanbakhsh et al. [4] experimentally investigated the mechanical properties of concrete with the partial replacement of coarse aggregate by FRP needles which were produced by cutting 6 mm diameter glass fiber-reinforced polymer (GFRP) reinforcing bars into 100 mm lengths. It was found from their study that due to the presence of FRP needles, even though the compressive strength of concrete decreased slightly, the splitting tensile strength of the concrete increased by 22-33%. In addition, the total energy absorbed (i.e., defined as the area under the load-displacement curve up to a specific displacement, which is either the final displacement reached in the test or another suitably chosen displacement) by the concrete specimen in either compression or tension was significantly increased as a result of the fact that the incorporated FRP needles inhibited the crack development, thus enhancing the deformability

of the specimen. Yazdanbakhsh et al. [5] conducted a similar study as Yazdanbakhsh et al. [4], except that they used FRP rectangular (6 mm by 6 mm by 100 mm) needles cut from a decommissioned wind turbine blade made of GFRP. From their study, it was found that although the incorporation of FRP needles did not significantly enhance the compressive, tensile and flexural strengths of concrete, it resulted in a notable increase in the total energy absorbed due to the enhanced deformability. Dong et al. [6] experimentally investigated the mechanical properties of seawater sea-sand concrete with its coarse aggregate partially replaced by FRP needles which were produced by cutting basalt fiber-reinforced polymer (BFRP) reinforcing bars. Their study found that due to the incorporation of FRP needles, even though the compressive strength of concrete reduced by up to 10%, the splitting tensile strength of concrete increased by 4-32%, and the flexural strength of concrete increased by 6-14%. In addition, the incorporation of FRP needles in seawater sea-sand concrete resulted in significant increases in the total energy absorbed because of the enhanced deformability. In addition, Yazdanbakhsh and Tian [7] conducted an experimental study on the shear behavior of small RC beams incorporating GFRP needles. The results showed that the GFRP needles enhanced the shear capacity of the small beams by 20-40%.

To verify the effectiveness of partial replacement of coarse aggregate of concrete with FRP needles in enhancing the structural performance of large-scale structural members, this paper presents the results of the first experimental investigation into the effect of GFRP needles as coarse aggregate partial replacement in concrete on the shear behavior of large-scale reinforced concrete (RC) beams. The GFRP needles, as part of the coarse aggregate, were expected to enhance the shear strength and ductility of the RC beam as they limit the opening and growth of shear or flexural-shear cracks, thus improving aggregate interlock and the dowel action of the flexural reinforcement.

2. EXPERIMENTAL PROGRAM

2.1 Specimen details

Ten large-scale RC beam specimens with a cross-section of 250 mm × 450 mm and a total length of 2,600 mm were tested with the details shown in Fig. 1. Three deformed steel bars of 32 mm in diameter were used as the primary tension reinforcement (reinforcement ratio ρ_s =2.4%), and two deformed steel bars of 12 mm in diameter were used as top support bars in the compression zone. Four stirrups, which were formed from smooth steel bars of a small diameter (10 mm), were used to facilitate the fabrication of steel cages. These four stirrups were located at the two supports and the two loading points, respectively, where shear cracks were not expected to occur, and the presence of these stirrups was expected to have a negligible effect on the shear behavior of the beam specimens. Stirrups of 10 mm in diameter at a spacing of 100 mm were provided in the left half of the beam so that the shear capacity of the left shear span was much larger than that of the right shear span. Such an arrangement of stirrups was to ensure that the shear failure of the beam would occur in the right half (i.e., the critical half). The concrete cover (from the beam soffit to the outer surface of tension steel bars) was 34 mm, leading to an effective depth of 400 mm for the test beams. The shear span-to-effective depth ratio (λ) (i.e., shear span/effective depth) adopted in this study was 2.0, providing a shear span of 800 mm. With such a shear span-to-effective depth ratio, the test specimens were expected to fail by crushing or splitting of the compression strut (i.e., a failure of arching action), in which an efficient arching action can be developed. It is believed that the total amount of absorbed energy can be enhanced by the incorporation of GFRP needles, as demonstrated by the tests on small cylindrical specimens presented in Yazdanbakhsh et al. [4]. It should be noted that the beneficial effects of incorporating GFRP needles on the structural performance are also expected to exist in more slender beams.

The test parameters examined in this study were the volume replacement ratio of coarse aggregate (v_n) and the surface type of GFRP needles. FRP needles were incorporated in concrete to replace 0%, 5% or 10% of coarse aggregate by volume. Smooth pultruded GFRP rods or helically wrapped GFRP rebars were used to produce needles, in order to study the effect of bond between FRP needles and concrete on the behavior of beams. Smooth pultruded GFRP rods of 6 mm in diameter and helically wrapped GFRP rebars of 7 mm in diameter were cut into needles of 100 mm in length (Fig. 2), which was the length of the needles used by Yazdanbakhsh et al. [7].

The ten test beams were divided into five pairs. Each pair included two companion beams. Further details of the test beams are given in Table 1. A beam specimen name consists of three character sets: set 1 is a letter-number combination (V0, V5 or V10) that represents the volume replacement ratio of coarse aggregate (i.e., 0% for the control specimens without FRP needles, 5% and 10% respectively); set 2 comprising two letters (CB, SM or HW) stands for the control beams, beams with smooth needles or beams with helically wrapped needles; and the last letter, being “a” or “b”, is used to differentiate two companion specimens. For example, Specimen V5SMa is the first identical beam in which the volume replacement ratio of coarse aggregate with smooth GFRP needles is 5%.

2.2 Material properties

2.2.1. Steel bars

The tensile properties of steel bars used in the present study were obtained through tensile tests according to the British standard BS-18 [8]. These steel bars included the deformed steel bars of 32 mm and 12 mm in diameter and smooth steel bars of 10 mm in diameter. For each

kind of steel bars, three specimens were prepared and tested. The average yield stress, ultimate stress and elastic modulus of each kind of steel bars are listed in Table 2.

2.2.2. GFRP rods/bars

The smooth pultruded GFRP rods and helically wrapped GFRP rebars used in this study were both produced by the same company and made from the same glass fiber and resin (unsaturated polyester resin). The mechanical properties of smooth pultruded GFRP rods were obtained though standard tensile tests according to ASTM D3916 [9], while the standard tensile tests on helically wrapped GFRP rebars were conducted in accordance with ASTM D7205 [10]. For tensile testing, the GFRP rebars were potted in metal sleeves per ASTM D7205 [10] using a polymer grout, and the GFRP rods were tested with end V-grips. For each kind of GFRP bars/rods, five specimens were prepared and tested, with a loading rate of 2.5 mm/min, following ASTM D3916 [9] and ASTM D7205 [10]. The deformation was measured using an extensometer installed at the mid-height of the bar. The stress-strain curves of the GFRP bars/rods are shown in Fig. 3, and the average ultimate stress and elastic modulus of the GFRP bars/rods are listed in Table 2.

Burn-out tests were conducted according to ASTM D2584 [11] to determine the mass and the volume fractions of fibers for both the smooth and helically wrapped GFRP needles. For each kind of GFRP needles, five specimens were prepared and tested. The photos of smooth/helically wrapped GFRP needles after a burn-out test are shown in Fig. 4 and the average burn-out test results are also listed in Table 2. It is evident from Table 2 that the mass/volume fraction of the helically wrapped GFRP needles is larger than that of the smooth needles, which led to their higher values of ultimate stress and elastic modulus than the smooth GFRP needles.

2.2.3. Concrete

The concrete for casting the beams was ordered from a local ready-mixed concrete supplier. The needles were mixed into the concrete at the plant. The mix proportions of the normal concrete without needles were provided by the supplier and the target concrete cube compressive strength was 40 MPa. The mix proportions and slump value of each batch of concrete are shown in Table 3. Fly ash and mineral powder (product of crushing the ore) were added to increase the workability of concrete. The water cement ratio (W/C) of the concrete was 0.43. As can be seen from Table 3, due to the presence of FRP needles, the slump reduced from 60 mm for the control batch to about 30 mm for the batches with FRP needles.

Flexural strength of small concrete beams

For each batch of concrete, three small beams with the dimensions of 150 mm in width and depth × 550 mm in length were tested following ASTM C1609 [12] to obtain their flexural strength. The span (l) of the small beams was 450 mm. All small beams failed in flexure due to the formation and development of a major flexural crack at the mid-span. The typical failure modes of the control small beams and the small beams with GFRP needles are shown in Fig. 5. After the test, a control small beam became two separate pieces (Fig. 5a), while a small beam with GFRP needles remained as one piece (Fig. 5b).

The load-deflection curves of the small beams are shown in Fig. 6, and the key test results are listed in Table 4, in which F_s is the ultimate load; f_s is the flexural strength of a small beam, which is equal to $F_s l/b_s d_s^2$, where l is the span, and b_s and d_s are the width and depth of the small beam, respectively; f_{sm} is the mean value of f_s; E_s is the total energy absorbed; and E_{sm} is the mean value of E_s. As can be seen from Fig. 6 and Table 4, enhancements of 19.3% and

48.1% in the flexural strength of small beams were obtained by replacing 5% and 10% of the coarse aggregate in volume with smooth needles (i.e., Batches 2 and 3). The average flexural strengths of small beams of Batches 4 and 5, in which the coarse aggregate was replaced by helically wrapped needles at 5% and 10% in volume, are respectively 7.4% smaller and 9.4% larger than that of the control group (i.e., Batch 1 without GFRP needles). Furthermore, the total energy absorbed (i.e., up to 4.5 mm of the mid-span deflection for small beams) of different batches of small beams (i.e., the area under the load-deflection curve from 0 to 4.5 mm of the mid-span deflection) are calculated based on Fig. 6 and the results are listed in Table 4. The areas under the load-deflection curves shown in Fig. 6 can be approximatively divided into two or three trapezoids and the total energy absorbed equals to the sum of the areas of the trapezoids. It can be seen from Table 4 that the average values of the total energy absorbed of different batches of small beams with FRP needles are larger than that of the control small beams without FRP needles by 262.7%-416.1%.

Splitting tensile strength of concrete cylinders

For each batch of concrete, three cylinder specimens with the dimensions of 150 mm in diameter × 300 mm in height were tested following ASTM C496 [13] to obtain their splitting tensile strengths. The typical failure modes of both control cylinders and cylinders with FRP needles under splitting tension are shown in Fig. 7. After the splitting tensile test, a control cylinder was broken into two separate pieces (as shown in Fig. 7a), while a cylinder with FRP needles remained as one piece (as shown in Fig. 7b).

The test results of cylinders under splitting tension are listed in Table 5. As can be seen from Table 5, the average splitting tensile strengths of cylinders of Batches 2 and 3, in which the coarse aggregate was partially replaced by smooth needles, are larger than the average

splitting tensile strength of the control cylinders by 13.1 and 22.8%, respectively; the average splitting tensile strength of cylinders of Batch 4, in which the coarse aggregate was replaced by helically wrapped needles at 5% in volume, is smaller than that of the control cylinders by 4.7%, while the average splitting tensile strength of cylinders of Batch 5, in which the coarse aggregate was replaced by helically wrapped needles at 10% in volume, is larger than that of the control cylinders by 2.8%. As the displacement of the loading machine could not be acquired, the load-deflection curves of these cylinders under splitting tension were not obtained. However, it can be deduced from the failure modes of control cylinders and cylinders with FRP needles (Fig. 7) that due to the incorporation of FRP needles, the total energy absorbed by the concrete specimen under splitting tension was enhanced significantly.

Compressive strength of cylinders

For each batch of concrete, another three cylinder specimens were tested following ASTM C39 [14] to obtain their compressive strengths and following ASTM C469 [13] to obtain their elastic moduli and Poisson's ratios. Two strain gauges of 100 mm in gauge length were vertically attached at the mid-height of each specimen to measure its axial strains, and another two strain gauges of 80 mm in gauge length were circumferentially attached at the mid-height of each specimen to measure its hoop strains. The compressive load was applied until the load decreased to 20% of the ultimate load of the cylinder. Fig. 8 shows the failure modes of all the cylinder specimens for compression tests, which indicates that the specimens with a larger volume of FRP needles (Batches 3 and 5) developed wider and deeper cracks and had more concrete blocks spalling from the specimen at the final stage of the loading process. This is because these two batches of specimens experienced a larger axial deformation and absorbed a higher amount of total energy at the final stage of the loading process.

The stress-strain curves of the cylinders under compression are shown in Fig. 9, and the key results are listed in Table 6. Similar to other fibrous products (e.g., steel fibers), there are two distinct mechanisms that result from the addition of GFRP needles: (1) the added needles limit the growth of cracks under compressive loading as a result of the bridging effect; and (2) defects between needles and concrete are introduced by the addition of needles, especially when the needle volume fraction exceeds a certain value. The former mechanism is beneficial to the strength and deformability of concrete under compressive loading, while the later results in a degradation of compressive strength of concrete [15]. The resulting effect of the addition of needles depends on the competing process of these two mechanisms, which are affected by the needle volume fraction as well as the mechanical properties of needles. As can be seen from Table 6, enhancements of 23.7% and 5.9% were achieved in the compressive strength by replacing 5% (Batch 2) and 10% (Batch 3) of the coarse aggregate with smooth GFRP needles respectively, while the average compressive strengths of cylinders of Batches 4 and 5, in which 5% and 10% of the coarse aggregate in volume were replaced with helically wrapped needles, are lower than that of the control batch by 8.9% and 12.6% respectively. The helically wrapped needles had rougher surfaces and thus are expected to have introduced more defects than smooth needles. The defects between needles and concrete may be effectively eliminated through vibration in the concrete casting process in practice, but this is difficult to realize in such relatively small specimens as the needles are unable to move around easily. As indicated in Table 6, the presence of helically wrapped and smooth needles enhances the total energy absorbed by the cylindrical specimens, and the enhancement becomes more significant when a larger percentage of coarse aggregate is replaced by the FRP needles. The largest amount of energy absorbed among all the five batches was observed in Batch 3. The enhanced amount of total energy absorbed by the cylindrical specimens due

to the addition of GFRP needles may partially explain the increase in the amount of the total energy absorbed by the large-scale RC beams. Most of these beams exhibited shear-compression failure in the present study, which is highly dependent on the compressive behavior of concrete.

Compressive strength of cubes

For each batch of concrete, three cubes with a side length of 150 mm were tested following Chinese code GB/T 50081 [16] to obtain their compressive strength. The failure modes of all cubes under compression are shown in Fig. 10.

The test results of cubes under compression are listed in Table 7. As can be seen from Table 7, the average compressive strengths of cubes of Batches 2 and 3, in which the coarse aggregate was partially replaced by smooth needles, are larger than the average compressive strength of the control cubes by 1.8% and 8.4% respectively, while the average compressive strengths of cubes of Batches 4 and 5, in which the coarse aggregate was partially replaced by helically wrapped needles, are smaller than the average compressive strength of the control cubes by 7.2% and 7.8% respectively.

Summary of the material test results of concrete

The material properties of the five batches of concrete are summarized in Table 8. It should be noted that the splitting tensile strength results of cylinders with helically wrapped needles do not agree with the observations made by Yazdanbakhsh et al. [4]. This may be due to the differences in the helically wrapped needles used in the two test series. The helically wrapped needles used in Yazdanbakhsh et al. [4] were sand-coated and obtained from a major supplier of GRFP rebars with many years of experience while those used in the present study were not.

Yazdanbakhsh et al. [4] did not test smooth rods. An increase of 32% was observed in the splitting tensile strength by Dong et al. [6] when 20% of the coarse aggregate was replaced with deformed BFRP needles of 10 mm in diameter and 100 mm in length. However, the enhancement in the splitting tensile strength was just 2% for concrete with a 15% volume replacement ratio of BFRP needles. It seems surprising that such a 5% difference in the replacement ratio of BFRP needles led to a relatively large difference in the splitting strength enhancement. In Yazdanbakhsh et al. [5], the splitting tensile strength, however, decreased by 0-14% with the partial replacement of coarse aggregate using smooth or grooved needles cut from wind blade shells. This may have been due to the poor tensile strength of the FRP needles and thus a weak bridging effect. In the burn-out tests presented in Yazdanbakhsh et al. [5] the glass fibers were perpendicular to the needle axis in the majority of the needles, and this resulted in the relatively poor tensile strength of the needles in their study. Clearly, if the FRP needles have good mechanical properties, the addition of needles into concrete is beneficial to the toughness under compression and bending as well as the splitting tensile strength of concrete. The presence of needles in concrete may therefore improve the structural performance of some structural elements under a variety of loading conditions (e.g., bending, shear, punching and torsion).

2.3 Large-scale beam test set-up and instrumentation

The layout of LVDTs and strain gauges is shown in Fig. 11. The deflections of beam specimens were measured using five LVDTs with one at each support, one at each loading point and one at the beam mid-span. Two strain gauges of 80 mm in gauge length were attached on the compression face of the mid-span of the specimens to measure the strain of the compressive concrete. One strain gauge of 5 mm in gauge length was installed onto one side of each tension steel bar at mid-span to measure the strains of the tension steel bars.

Four-point bending was used for testing all the large-scale beam specimens with the test set-up as shown in Fig. 12. The loads were applied through two hydraulic jacks, both of which were connected to one single manually-operated pump, to ensure simultaneous loading from the two jacks. A load cell was installed under each loading point to measure the precise load at the loading point. The loading rate was quasi-static with the typical time taken to complete each test being about 4 hours. A data acquisition system capable of digitally recording and storing load, deflection and strain data at a sampling frequency of 1 Hz was used in the tests.

3. FAILURE MODES

All ten beams failed by shear due to the formation of a main diagonal crack in the right shear span (the shear span without stirrups) which linked the right loading point and the right support. The failure of all ten beams occurred in a brittle manner, with different levels of noise made by beams with different volumes of FRP needles. The two control beams (V0CBa and V0CBb) failed with a very loud noise, while the four beams with 10% of coarse aggregate in volume replaced by FRP needles (V10SMa, V10SMb, V10HWa and V10HWb) had very little noise when they failed; the noise made by the four beams with 5% of coarse aggregate in volume replaced by FRP needles (V5SMa, V5SMb, V5HWa and V5HWb) when they failed was less than that made by the two control beams but more than that made by the four beams with 10% of coarse aggregate in volume replaced by FRP needles. The loading process was not stopped when the beams failed, but was continued until the deflection was large enough or the loading header was out of perpendicular alignment so that it would have been hazardous if the loading process was continued. It should be noted that even though all ten beams failed by shear, two different crack patterns were seen (as shown in Fig. 13): (1)

Crack Pattern I: the main diagonal crack was at about 45 degrees to the horizontal line. The 45-degree crack extended from the loading point to the top of the tension rebars. It then extended along the top of the rebars to the right support (Fig. 13a); and (2) Crack Pattern II: the main diagonal crack was at approximately 30 degrees to the horizontal line and extended from the loading point directly to the right support (Fig. 13b). Only two of the ten beams exhibited Crack Pattern II (V5SMb and V10HWa) while the other eight beams all exhibited Crack Pattern I. This situation that two beams of the same batch (e.g. V5SMa and V5SMb) exhibited different crack patterns may be due to the statistical variability of reinforced concrete specimens, especially in the case of the short shear spans used in this investigation.

After the testing, the ends of the failed beam specimens with needles were broken off along the main shear crack to see the distribution and condition of the needles, as shown in Fig. 14, in which Specimens V10SMb and V10HWb were taken as examples. It is evident from Fig. 14 that there were a number of FRP needles across the main shear crack, almost all of which were pulled out from the concrete. The needles at the main shear crack improved the performance of RC beams by directly resisting the shear force and enhancing the aggregate interlock. In addition, the better bond properties between the helically wrapped needles and the concrete led to a greater beneficial effect than that offered by smooth needles as indicated in Fig. 14.

4. STRUCTURAL RESPONSES OF BEAMS

4.1 Load-deflection curves

The load-deflection curves of the ten test beam specimens are shown in Fig. 15, in which the vertical axis shows the shear force (half of the total beam load, averaged from the readings of the two load cells) and the horizontal axis shows the mid-span deflection. The shapes of the

load-deflection curves of all ten beams are similar. Before the flexural cracking of the bottom concrete, the load increased linearly with the deflection; after the flexural cracking of the concrete, the load still increased nearly linearly with the deflection but at a slightly smaller slope (i.e. stiffness); and after the ultimate load was reached, the load dropped suddenly to a relatively low level, and then the load only showed a very slight decrease with the deflection (can be seen as a plateau). The plateau can be mainly attributed to dowel action of the main rebars.

4.2 Strains in the concrete and the steel bars

An examination of the strain readings in the concrete and steel bars revealed that the general features of strain development (i.e., curves of strain development) are similar for all specimens, so only Specimen V10SMb is discussed herein as an example to demonstrate the development of strains in the compressive concrete and the tension steel bars during the loading process. The curves of strains in the compressive concrete and the tension steel bars versus the mid-span deflection of the beam are shown in Fig. 16. As can be seen from Fig. 16, the shapes of strain-deflection curves of the compressive concrete and the tension steel bars are quite similar to those of the load-deflection curves of beam specimens shown in Fig. 15. The strains of compressive concrete and tension steel bars of the beam specimens at the ultimate load are listed in Table 9. It can be seen from Table 9 that the strains of the compressive concrete and the tension steel bars at ultimate load are positively correlated with the ultimate loads of the beam specimens. The tension steel bars in all beam specimens did not yield (the yield strain of tension steel bar was 2384 $\mu\varepsilon$), and the compressive concrete in all beam specimens was far from being crushed (the ultimate strain of concrete in compression was about 3300 $\mu\varepsilon$). Moreover, it can be seen from Fig. 16 and Table 9 that the magnitudes of compressive strains in the concrete and tensile strains in the steel bars are

approximately equal, which indicates that the neutral axis was at about the mid-height of the beam. This was a result of the high tension steel reinforcement ratio (i.e., 2.4%).

4.3 Analysis of test results

The main test results of the beam specimens are listed in Table 9. It can be seen from Table 9 that the average shear capacity of the control beams (Batch 1) is 350 kN. According to the Chinese design code for concrete structures [17], the shear capacity of RC beams without stirrups (V) can be calculated as follows:

$$V=\frac{1.75}{\lambda+1} f_t b h_0 \tag{1}$$

where λ is the shear span-to-effective depth ratio (if λ<1.5, let λ=1.5; if λ>3, let λ=3); f_t is the tensile strength of concrete; b is the width of the beam; and h_0 is the effective depth of the beam.

According to the American design code for concrete structures [18], the shear capacity of RC beams without stirrups (V) can be calculated as follows:

$$V=（0.1578\sqrt{f_c^{'}}+17.25\rho_w \frac{V_u h_0}{M_u})bh_0 \tag{2}$$

where $f_c^{'}$ is the cylinder compressive strength of concrete; ρ_w is the ratio of A_s to bh_0, where A_s is the area of longitudinal tension reinforcement; V_u is the shear force at the section; and M_u is the moment at the section.

Different from ACI-318 [18] which provides an overall resistance factor for the structural member (0.75), the Chinese code [17] specifies partial safety factors for the materials (e.g., the partial safety factor for concrete is 1.4). The shear capacity of the control beams

calculated based on GB-50010 [17] is 154 kN (110 kN with the partial safety factor of concrete) and that calculated based on ACI-318 [18] is 136 kN (102 kN with the 0.75 resistance factor), which is much smaller than the test result (350 kN on average). The calculated shear capacity of the control beams is about 40% of the actual shear capacity, which is reasonable due to the conservative nature of design code provisions for shear failure of RC beams.

As indicated in Table 9, the variation in the failure mode led to a significant difference in the ultimate load of the companion beams. More specifically, the beams which failed by and exhibited Crack Pattern II (e.g., V5SMb and V10HWa) had ultimate loads that are smaller by about 20% than those of their companion beams which failed with Crack Pattern I (i.e., V5SMa and V10HWb). Such variations in the failure mode and the ultimate load are not surprising due to the well-known scatter of shear failure loads of deep RC beams [19]. Moreover, replacing coarse aggregate partially by smooth needles did not increase the shear capacity of the beam (the average shear capacity of the two beams decreased by 10% when 5% of the coarse aggregate in volume was replaced by smooth needles), while replacing 5% and 10% of the coarse aggregate by helically wrapped needles increased the shear capacities of the beams by 8.3% and 10.3% respectively. This appears to suggest that the surface type of GFRP needles has a significant effect on the shear capacity of the beam. As can be seen from Fig. 14, for either smooth needles or helically wrapped needles, almost all of the needles were pulled out from the concrete when the width of the main shear crack was large enough, which implies that the bond between the needles and the concrete may have played a significant role in the present tests. The volume replacement ratio of coarse aggregate also affects the shear capacity of the beam. For both smooth needles and helically wrapped needles, a larger

volume replacement ratio of coarse aggregate leads to a larger shear capacity of the beam, but the additional shear capacity gain is not in proportion to the added amount of FRP needles.

4.4 Energy absorption

The amounts of total energy absorbed by the beam specimens were calculated and are listed in Table 10. The total amount of absorbed energy is defined as the area under the load versus mid-span deflection curve up to 27 mm of the mid-span deflection. This specific value was chosen based on the consideration that among all the RC beam specimens, Specimen V0CBa had the smallest mid-span deflection at the end of the loading process, which was a little over 27 mm. The amount of absorbed energy is calculated as the area under the load versus mid-span deflection curve when the mid-span deflection is between 0 mm and 27 mm because the minimum mid-span deflection of the test beams when the loading process was stopped was 27 mm (Specimen V0CBa). Table 10 shows that the average amount of total energy absorbed by the two beams of each batch with FRP needles is larger than that of the two control beams by 33.2%-40.3%. With the same volume replacement ratio of coarse aggregate, the beams with helically wrapped needles absorbed more energy than the beams with smooth needles; and with a larger volume of coarse aggregate replaced by either smooth needles or helically wrapped needles, the total energy absorbed by the beams increased. Among all the five batches of beams, beams of Batch 5, in which 10% of the coarse aggregate in volume was replaced by helically wrapped needles, absorbed the largest amount of total energy. The differences in the noise made by the beams at failure support this conclusion.

4.5 Comparison between test results of small specimens and large-scale RC beam specimens

In terms of the material properties of concrete, including the flexural strength, splitting tensile strength and compressive strength, concrete with coarse aggregate partially replaced by smooth needles performed better than that by helically wrapped needles. However, in the large-scale RC beam specimens, replacing the coarse aggregate partially by smooth needles did not increase the shear capacity of the beam. Replacing the coarse aggregate partially by helically wrapped needles increased the shear capacity of the large-scale beams by about 8% or 10% on average for volume replacement ratios of 5 and 10% respectively. As has been discussed in the introduction, the present study aimed at investigating the influence of FRP needles with respect to strengthening and toughening the compression struts against failures controlled by splitting, for which the results from cylinders have offered encouraging evidence, even though large struts may behave differently. The test results appear to indicate that the bond behavior between the FRP needles and the concrete is significant for the shear behavior of large-scale beam specimens, but not as significant in the small beam specimens. It can also be concluded from the test results that the coarse aggregate of RC beams can be partially replaced with GFRP needles, without negative effects on their strength. Furthermore, GFRP needles may serve to offset the size effect in RC beams without stirrups (or with light shear reinforcement) by controlling crack opening and growth [20,21].

5. CONCLUDING REMARKS

Cutting FRP waste into FRP needles for use as partial replacement of coarse aggregate in concrete may be a solution to address the environmental concern caused by the increasing amount of FRP waste. A total of 10 large-scale RC beams without stirrups in the critical region were tested in the present study to study the effect of such coarse aggregate partial

replacement on the shear capacity of RC beams. For this purpose, three different replacement ratios (i.e., replacement of 0%, 5% or 10% in volume of the coarse aggregate with FRP needles) and two surface types (i.e., smooth and helically wrapped) were considered in this study. Based on the test results and discussions, the following conclusions can be drawn:

1) All large-scale RC test beams failed in shear in a brittle manner with the ductility being slightly enhanced by the partial replacement of coarse aggregate with GFRP needles. Typical shear failure modes (anchorage failure or strut failure) were observed for the test beams;
2) An enhancement of about 8%-10% in the shear capacity was achieved in large-scale RC beams with helically wrapped needles, while beams with smooth needles showed a slight reduction in the shear capacity. These observations demonstrate that the addition of GFRP needles has no detrimental effect, and indeed may have a beneficial effect, on the shear capacity of the beam for some cases;
3) The presence of FRP needles increased the amount of total energy absorbed by the large-scale RC beams by about 33%-40%. The increased energy absorption of RC beams due to the FRP needles is expected to be beneficial where dynamic loading is considered (e.g., earthquakes, impact, blast). This aspect is worthy of further investigations;
4) The bond behavior between FRP needles and concrete appears to be significant in the shear behavior of large-scale RC beam specimens, but not in small material test specimens. The bond behavior between GFRP needles and concrete is an important issue that should be investigated in future studies; and
5) The enhancement of shear capacity of large-scale RC beams by partially replacing the coarse aggregate with the GFRP needles adopted in the present study (6 mm in diameter and 100 mm in length) is not remarkable. The contribution of GFRP needles to the shear capacity of RC beams may have been obscured by the small shear span-to-depth ratio of

2.0. There may be an opportunity to optimize the needles for better performance. The increases in energy absorption and ultimate load in some beams are an encouraging sign. The influence of shape, size and surface properties of GFRP needles needs to be further examined in future studies.

ACKNOWLDGEMENTS

The authors gratefully acknowledge the financial support provided by the Hong Kong Research Grants Council (Project No: T22-502/18-R), The Hong Kong Polytechnic University (Project account code: 1-BBAG) and Guangdong University of Technology. Partial support for YT and LCB was provided by the US National Science Foundation under grant numbers 1345379, 1551018 and 1701694.

REFERENCES

[1] Yazdanbakhsh, A. and Bank, L.C. (2014). "A critical review of research on reuse of mechanically recycled FRP production and end-of-life waste for construction", *Polymers*, 6(6), 1810-1826.

[2] Oliveux, G., Dandy, L. and Leeke, G. (2015). "Current status of recycling of fibre reinforced polymers: Review of technologies, reuse and resulting properties", *Progress in Materials Science,* 72, 61-99.

[3] Ribeiro, M.C.S., Meira-Castro, A.C., Silva, F.G., Santos, J., Meixedo, J.P., Fiúza, A., Dienis, M.L. and Alvim, M.R. (2015). Re-use assessment of thermoset composite wastes as aggregate and filler replacement for concrete-polymer composite materials: a case study regarding GFRP pultrusion wastes", *Resources, Conservation and Recycling*, 104, 417-426.

[4] Yazdanbakhsh, A., Bank, L.C., Chen, C. and Tian, Y. (2017). "FRP-needles as discrete reinforcement in concrete", *Journal of Materials in Civil Engineering, ASCE*, 29(10), 04017175.

[5] Yazdanbakhsh, A., Bank, L.C., Rieder, K.A., Tian, Y. and Chen, C. (2018). "Concrete with discrete slender elements from mechanically recycled wind turbine blades", *Resources, Conservation and Recycling*, 128, 11-21.

[6] Dong, Z., Wu, G. and Zhu, H. (2019). "Mechanical properties of seawater sea-sand concrete reinforced with discrete BFRP-Needles", *Construction and Building Materials*, 206, 432-441.

[7] Yazdanbakhsh, A. and Tian, Y. (2019). "Shear performance of reinforced concrete beams incorporating stiff slender elements", *Construction and Building Materials*, 222, 263-277.

[8] BSI (1987). *Method for tensile testing of metals*, BS-18, London, U.K.

[9] ASTM (2008). *Standard test method for tensile properties of pultruded glass-fiber-reinforced plastic rod*, ASTM D3916, West Conshohocken, PA.

[10] ASTM (2011). *Standard test method for tensile properties of fiber reinforced polymer matrix composite bars*, ASTM D7205, West Conshohocken, PA.

[11] ASTM (2018). *Standard test method for ignition loss of cured reinforced resins*, ASTM D2584, West Conshohocken, PA.

[12] ASTM (2012). *Standard test method for flexural performance of fiber-reinforced concrete (using beam with third-point loading)*, ASTM C1609, West Conshohocken, PA.

[13] ASTM (2014). *Standard test method for static modulus of elasticity and Poisson's ratio of concrete in compression*, ASTM C469, West Conshohocken, PA.

[14] ASTM (2018). *Standard test method for compressive strength of cylindrical concrete specimens*, ASTM C39, West Conshohocken, PA.

[15] Li, V.C. (1992). "A simplified micromechanical model of compressive strength of fiber-reinforced cementitious composites", *Cement and Concrete Composites*, 14, 131-141.

[16] GB/T 50081 (2016). *Standard for test method of mechanical properties on ordinary concrete*, Architectural and Building Press, Beijing, China. (in Chinese)

[17] GB-50010 (2010). *Code for design of concrete structures*, Architectural and Building Press, Beijing, China. (in Chinese)

[18] ACI-318 (2014). *Building code requirements for structural concrete and commentary (ACI 318-14)*, ACI Committee 318, American Concrete Institute, Farmington Hills, MI.

[19] ACI-ASCE Committee 426 (1973). "The shear strength of reinforced concrete members", *Journal of the Structural Division*, 99(6), 1091-1187.

[20] Matta, F., El-Sayed, A.K., Nanni, A. and Benmokrane, B. (2013). "Size effect on concrete shear strength in beams reinforced with fiber-reinforced polymer bars", *ACI Structures Journal*, 110 (4), 617-628.

[21] Khodaie, S., Matta, F. and Alnaggar, M. (2019). "Discrete meso-scale modeling and simulation of shear response of scaled glass FRP reinforced concrete beams without stirrups", *Engineering Fracture Mechanics*, 216, 106486.

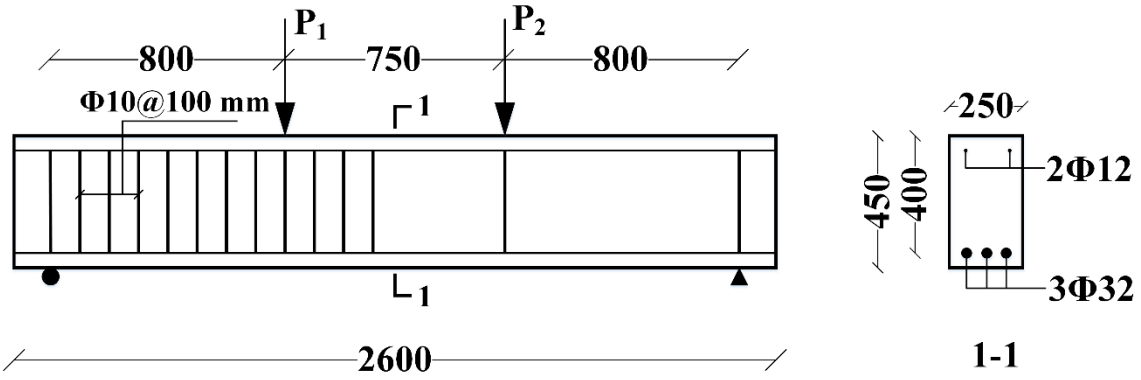

Figure 1. Details of the large-scale RC beam specimens (dimensions in mm)

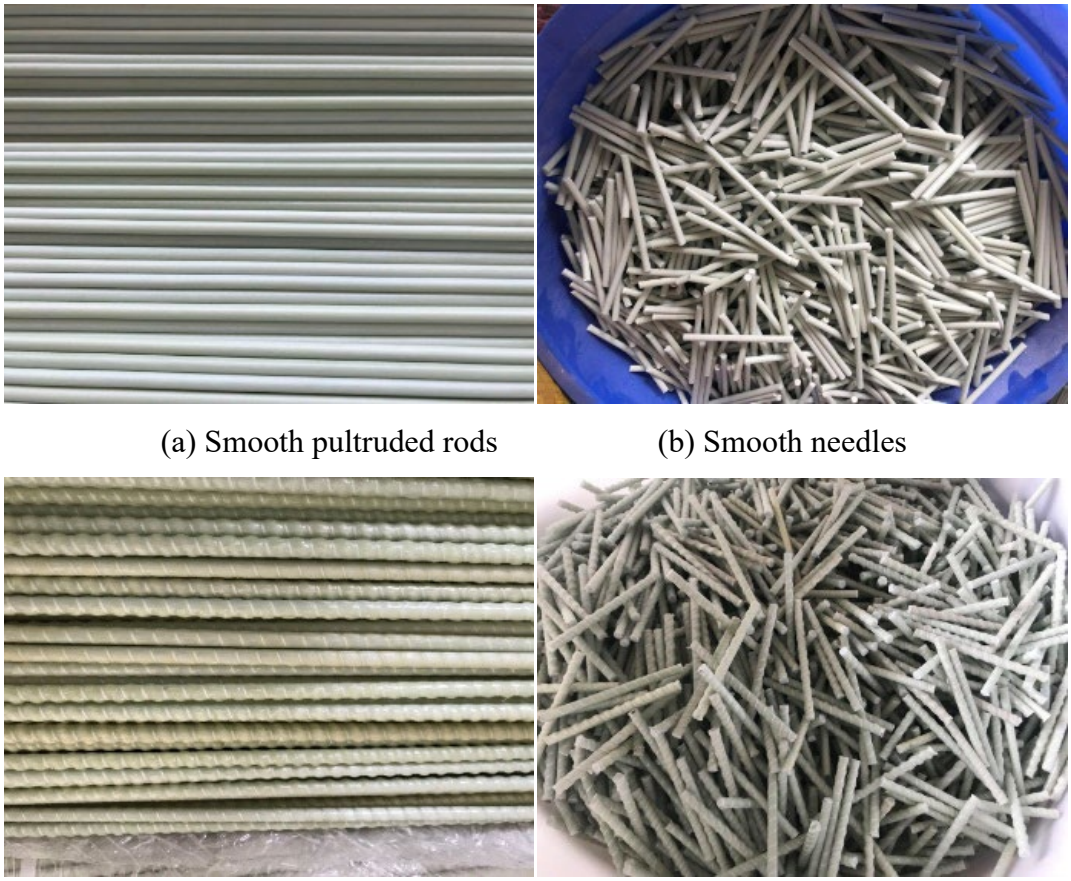

(a) Smooth pultruded rods (b) Smooth needles

(c) Helically wrapped rebars (d) Helically wrapped needles

Figure 2. GFRP needles cut from GFRP rods/rebars and used in the study

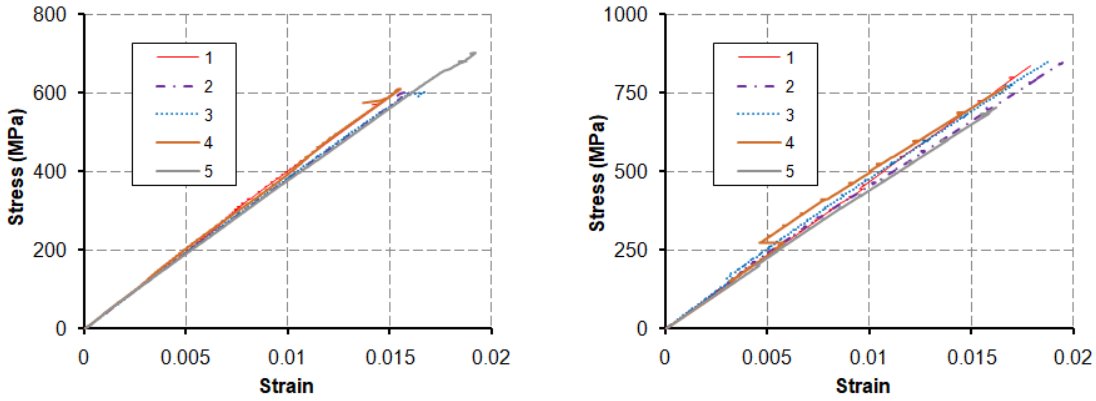

(a) Smooth pultruded rods (b) Helically wrapped rebars

Figure 3. Stress-strain curves of the GFRP rods/rebars used in the study

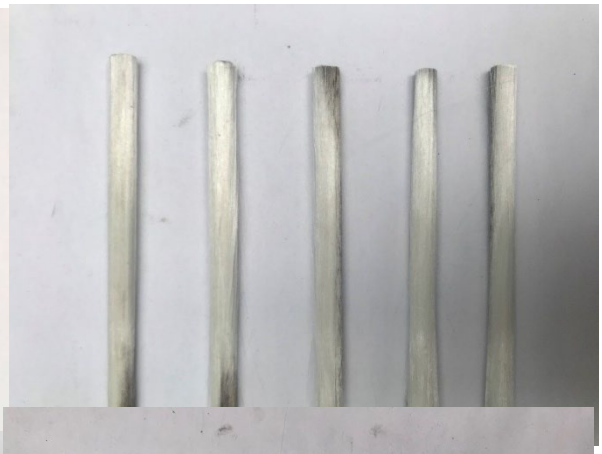

(Side face) (Fracture surface)

(a) Control small concrete beam

(Side face) (Bottom)

(b) Small concrete beam with GFRP needles

Figure 5. Failure modes of small concrete beams

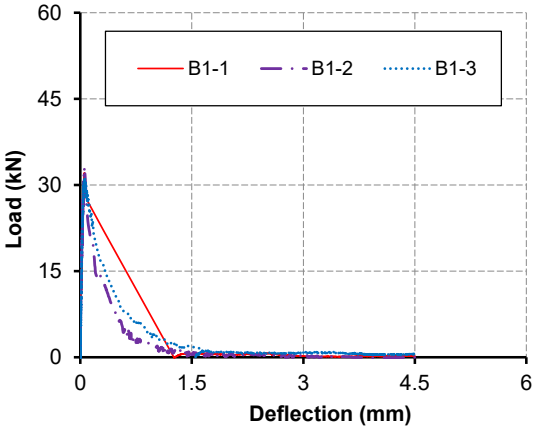

(a) Batch 1

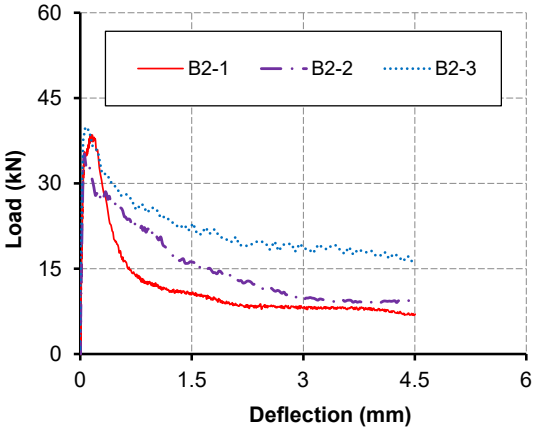

(b) Batch 2

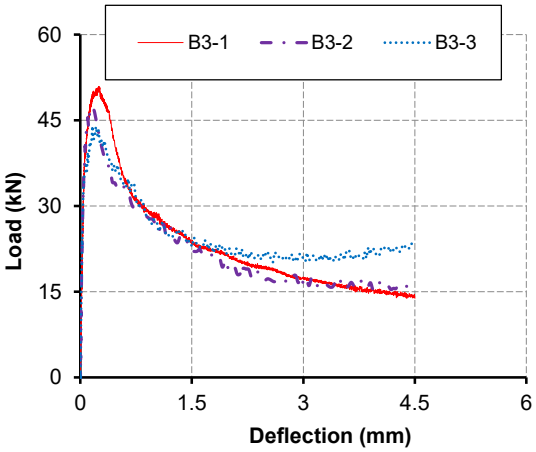

(c) Batch 3

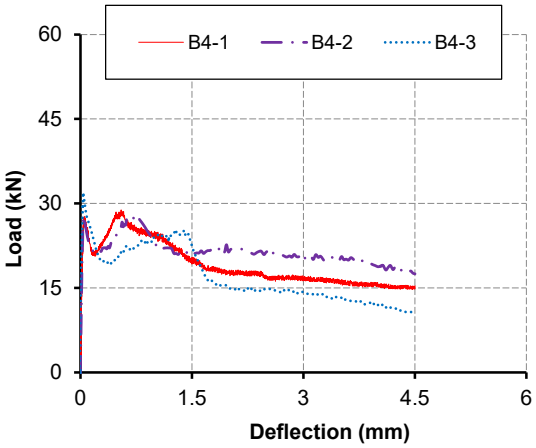

(d) Batch 4

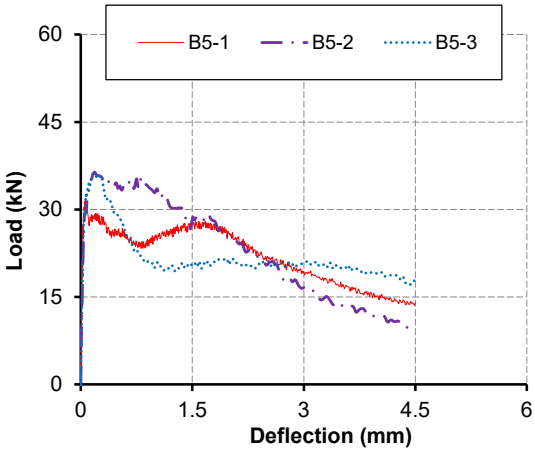

(e) Batch 5

Figure 6. Load-deflection curves of small concrete beams

(a) Control cylinder (b) Cylinders with GFRP needles

Figure 7. Failure modes of cylinders under splitting tension

(a) Batch 1

(b) Batch 2

(c) Batch 3

(d) Batch 4

(e) Batch 5

Figure 8. Failure modes of cylinders under compression

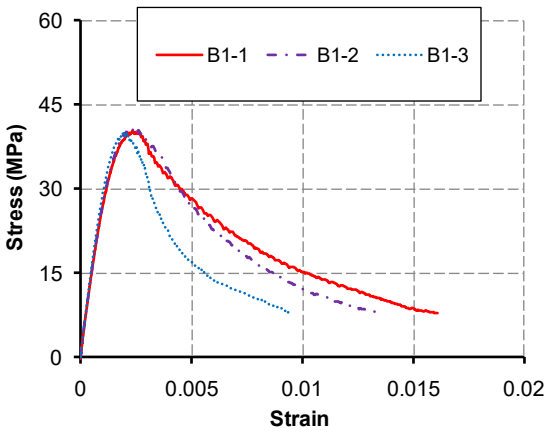

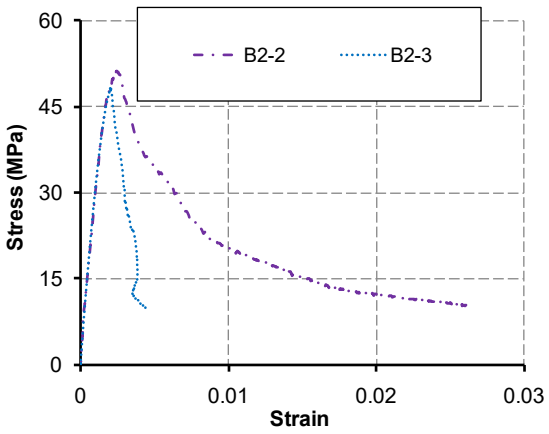

(Note: The data of Cylinder B2-1 was not acquired due to operation errors)

(a) Batch 1

(b) Batch 2

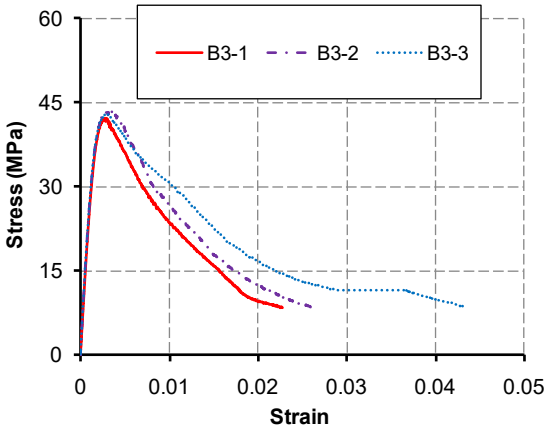

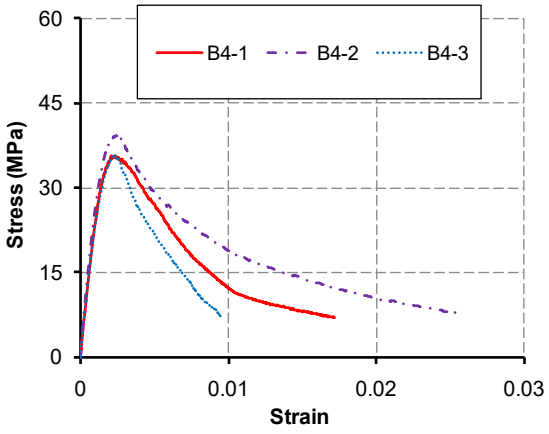

(c) Batch 3

(d) Batch 4

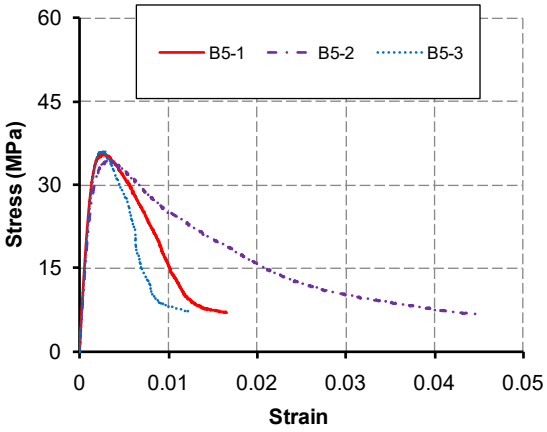

(e) Batch 5

Figure 9. Stress-strain curves of cylinders under compression

(a) Batch 1

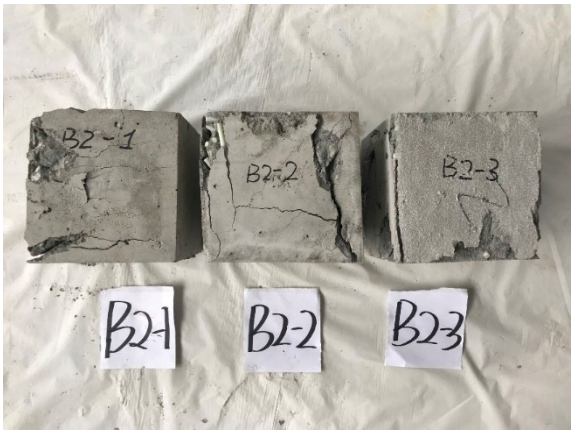

(b) Batch 2

(c) Batch 3

(d) Batch 4

(e) Batch 5

Figure 10. Failure modes of cubes under compression

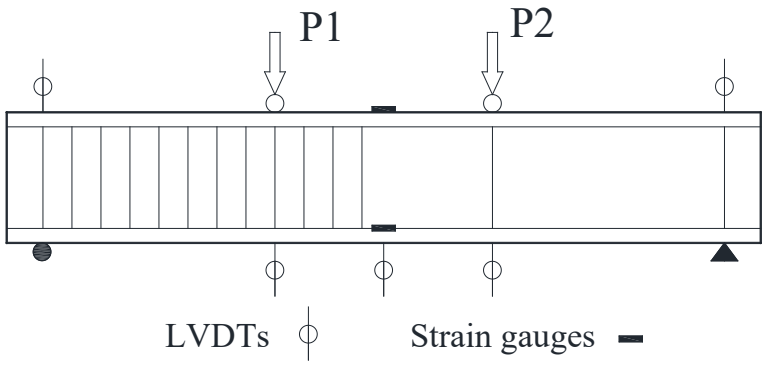

Figure 11. Layout of LVDTs and strain gauges in large-scale beam tests

Figure 12. Test set-up of the large-scale RC beam specimens

(a) Crack Pattern I (b) Crack Pattern II

Figure 13. Failure modes of the large-scale RC beam specimens

(a) V10SMb (b) V10HWb

Figure 14. Conditions of the needles along the main shear crack

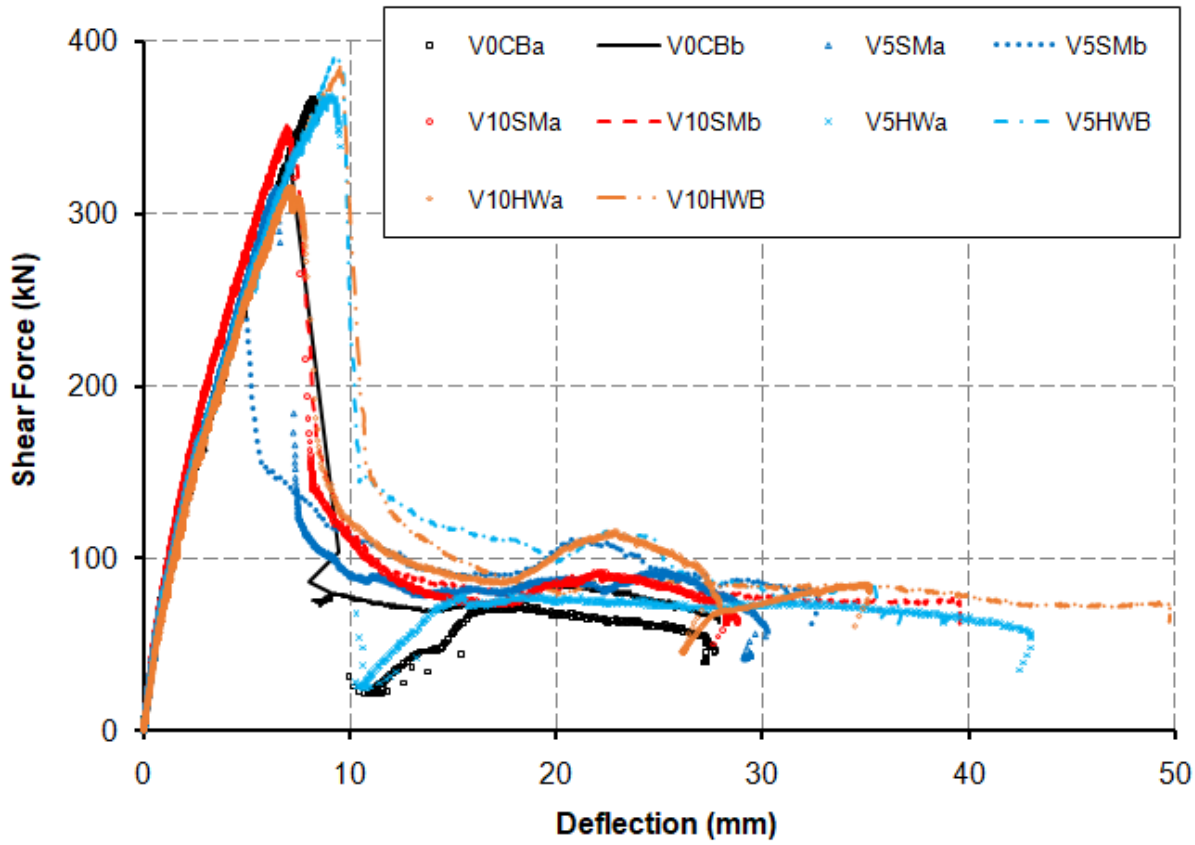

Figure 15. Load-deflection curves of the large-scale RC beam specimens

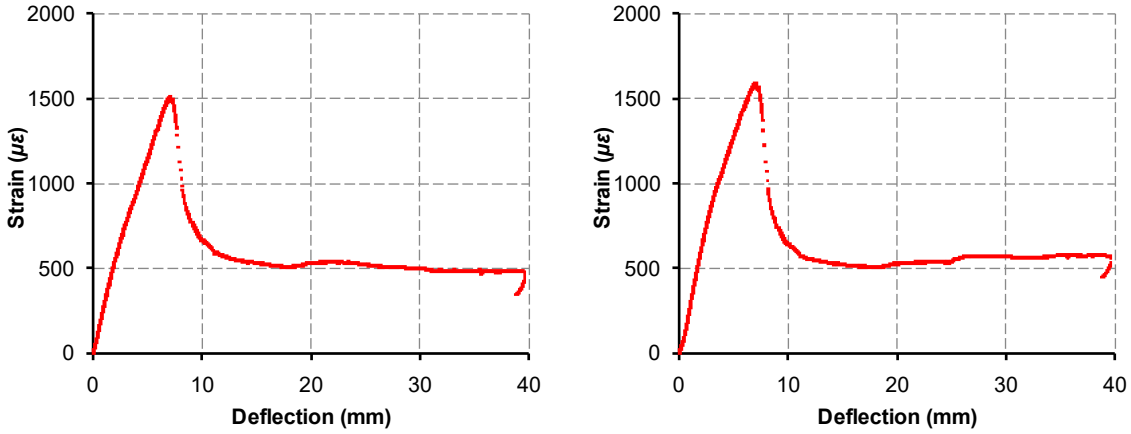

(a) Compressive concrete (b) Tension steel bars

Figure 16. Strains in the concrete and the steel bars of RC beam specimen V10SMb

Table 1. Details of large-scale RC beams

Batch	Specimen name	L (mm)	L_s (mm)	h (mm)	h_0 (mm)	b (mm)	λ	v_n (%)	Surface type of FRP needles
1	V0CBa	2350	800	450	400	250	2.0	0	-
	V0CBb							0	-
2	V5SMa							5	Smooth
	V5SMb							5	Smooth
3	V10SMa							10	Smooth
	V10SMb							10	Smooth
4	V5HWa							5	Helically wrapped
	V5HWb							5	Helically wrapped
5	V10HWa							10	Helically wrapped
	V10HWb							10	Helically wrapped

Note: L=clear span of specimen; L_s=shear span of specimen; h=beam depth; h_0=effective beam depth; b=beam width; λ=shear span-to-effective depth ratio; v_n=volume replacement ratio of coarse aggregate by FRP needles.

Table 2. Material properties of steel bars and GFRP rods/bars

Property	Steel bars of 32 mm in diameter	Steel bars of 12 mm in diameter	Steel bars of 10 mm in diameter	Smooth pultruded rods	Helically wrapped rebars
Yield stress (MPa)	459.9	381.6	345.1	-	-
Ultimate stress (MPa)	633.3	504.5	515.8	620.2	843.1
Elastic modulus (GPa)	192.9	190.1	205.2	39.4	46.1
Mass fraction of fiber (%)	-	-	-	69.5	78.7
Volume fraction of fiber (%)	-	-	-	50.1	62.0

Table 3. Mix proportions and slumps of concrete

Batch	Specimen name	v_n (%)	Surface type of needles	Coarse aggregate (kg/m^3)	Fine aggregate (kg/m^3)	Cement (kg/m^3)	Water (kg/m^3)	Fly ash (kg/m^3)	Mineral powder (kg/m^3)	Water reducer (kg/m^3)	GFRP needles (kg/m^3)	Slump value (mm)
1	V0CBa	0	-	1060	807	220	147	45	75	6.29	0	60
	V0CBb											
2	V5SMa	5	Smooth	1007	807	220	147	45	75	6.29	38	30
	V5SMb											
3	V10SMa	10	Smooth	954	807	220	147	45	75	6.29	76	28
	V10SMb											
4	V5HWa	5	Helically wrapped	1007	807	220	147	45	75	6.29	40	31
	V5HWb											
5	V10HWa	10	Helically wrapped	954	807	220	147	45	75	6.29	80	29
	V10HWb											

Table 4. Test results of small concrete beams

Batch	Specimen	Corresponding beam specimen	F_s (kN)	f_s (MPa)	f_{sm} (MPa)	Gain in f_{sm} due to FRP needles	E_s (J)	E_{sm} (J)	Gain in E_{sm} due to FRP needles
1	B1-1	V0CBa V0CBb	32.1	4.28	4.29	-	22.90	21.95	-
	B1-2		33.3	4.44			18.59		
	B1-3		31.2	4.16			24.37		
2	B2-1	V5SMa V5SMb	38.5	5.13	5.12	19.3%	57.03	79.62	262.7%
	B2-2		36.0	4.80			74.77		
	B2-3		40.7	5.43			107.07		
3	B3-1	V10SMa V10SMb	50.9	6.79	6.36	48.1%	109.42	113.29	416.1%
	B3-2		47.8	6.37			111.06		
	B3-3		44.4	5.92			119.39		
4	B4-1	V5HWa V5HWb	28.9	3.85	3.97	-7.4%	81.63	80.17	265.2%
	B4-2		28.6	3.81			87.38		
	B4-3		32.0	4.27			71.50		
5	B5-1	V10HWa V10HWb	32.0	4.27	4.69	9.4%	89.54	95.05	333.0%
	B5-2		36.6	4.88			104.26		
	B5-3		37.1	4.95			91.34		

Note: F_s=ultimate load; f_s=flexural strength of small beam=$F_s l/b_s d_s^2$, where l is the span, and b_s and d_s are the width and depth of the small beam specimen, respectively; f_{sm}=mean value of f_s; E_s=the total energy absorbed; E_{sm}=mean value of E_s.

Table 5. Test results of cylinders under splitting tension

Batch	Specimen	Corresponding beam specimen	f_{st} (MPa)	f_{stm} (MPa)	Gain in the splitting tensile strength due to FRP needles
1	B1-1	V0CBa V0CBb	3.76	3.60	-
	B1-2		3.80		
	B1-3		3.25		
2	B2-1	V5SMa V5SMb	3.63	4.07	13.1%
	B2-2		4.43		
	B2-3		4.16		
3	B3-1	V10SMa V10SMb	4.28	4.42	22.8%
	B3-2		4.31		
	B3-3		4.66		
4	B4-1	V5HWa V5HWb	3.48	3.43	-4.7%
	B4-2		3.35		
	B4-3		3.46		
5	B5-1	V10HWa V10HWb	3.62	3.70	2.8%
	B5-2		3.66		
	B5-3		3.83		

Note: f_{st}=splitting tensile strength of cylinder; f_{stm}=mean value of f_{st}.

Table 6. Test results of cylinders under compression

Batch	Specimen	Corresponding beam specimen	f_c (MPa)	f_{cm} (MPa)	E (GPa)	E_m (GPa)	μ	μ_m	E_c (J)	E_{cm} (J)	Gain in the compressive strength due to FRP needles	Gain in the absorbed energy due to FRP needles
1	B1-1	V0CBa V0CBb	40.4	40.5	29.7	30.4	0.16	0.18	2008.7	1616.6	-	-
	B1-2		40.8		29.4		0.17		1674. 3			
	B1-3		40.2		32.1		0.21		1166.91			
2	B2-1	V5SMa V5SMb	50.2	50.1	-*	31.2	-*	0.16		2420.6	23.7	49.7%
	B2-2		51.1		30.3		0.16		4188.7			
	B2-3		48.9		32.2		0.15		652.5			
3	B3-1	V10SMa V10SMb	42.2	42.9	26.9	28.0	0.16	0.17	2984.9	4107.6	5.9	154.1%
	B3-2		43.5		28.4		0.19		3489.8			
	B3-3		42.9		28.7		0.16		5848.1			
4	B4-1	V5HWa V5HWb	35.7	36.9	26.3	26.1	0.19	0.20	1901.56	2021.7	-8.9	25.1%
	B4-2		39.2		26.6		0.21		3134.4			
	B4-3		35.7		25.3		0.19		1029.0			
5	B5-1	V10HWa V10HWb	35.7	35.4	27.3	25.2	0.19	0.20	1830.2	2668.6	-12.6	65.1%
	B5-2		34.4		23.7		0.20		4805.3			
	B5-3		36.2		24.6		0.20		1370.3			

Note: f_c=compressive strength of cylinder; f_{cm}=mean value of f_c; E=modulus of elasticity in compression; E_m=mean value of E; μ=Poisson's ratio; μ_m=mean value of μ; E_c=total energy absorbed by the cylinder in compression; E_{cm}=mean value of E_c.

* The data of Cylinder B2-1 was not acquired due to operation errors.

Table 7. Test results of cubes under compression

Batch	Specimen	Corresponding beam specimen	f_{cu} (MPa)	f_{cum} (MPa)	Gain in the cube compressive strength due to FRP needles
1	B1-1	V0CBa V0CBb	50.8	49.8	-
	B1-2		48.8		
	B1-3		42.0*		
2	B2-1	V5SMa V5SMb	51.9	54.0	8.4%
	B2-2		52.5		
	B2-3		57.5		
3	B3-1	V10SMa V10SMb	51.7	50.7	1.8%
	B3-2		50.2		
	B3-3		50.3		
4	B4-1	V5HWa V5HWb	46.7	45.9	-7.8%
	B4-2		47.1		
	B4-3		43.8		
5	B5-1	V10HWa V10HWb	47.1	46.2	-7.2%
	B5-2		44.5		
	B5-3		47.0		

Note: f_{cu}=cube compressive strength of concrete; f_{cum}=mean value of f_{cu}.
*This result is deemed to be unreliable as the loaded surface was not a smooth surface.

Table 8. Summary of material properties of concrete (MPa)

Batch	Corresponding beam specimen	Flexural strength of small beams	Splitting tensile strength of cylinders	Compressive strength of cylinders	Compressive strength of cubes
1	V0CBa V0CBb	4.29	3.60	40.5	49.8
2	V5SMa V5SMb	5.12	4.07	50.1	54.0
3	V10SMa V10SMb	6.36	4.42	42.9	50.7
4	V5HWa V5HWb	3.97	3.43	36.9	45.9
5	V10HWa V10HWb	4.69	3.70	35.4	46.2

Table 9. Test results of large-scale RC beams

Batch	Specimen name	Crack pattern	Cracking load (kN)	Ultimate load (kN)	Strain of compressive concrete at ultimate load ($\mu\varepsilon$)	Strain of tension steel bars at ultimate load ($\mu\varepsilon$)	Residual load when the mid-span deflection reached 27 mm[(b)] (kN)	Mean value of ultimate load (kN)	Gain in ultimate load due to FRP needles
1	V0CBa	I	75	366	1541	2001	55	350	-
	V0CBb	I	75	333	1380	1648	67		
2	V5SMa	I	60	315	1256	1535	84	315[(c)]	-10.0%
	V5SMb	II	60	248	998	1180	90		
3	V10SMa	I	75	345	1506	-[(a)]	78	349	-0.3%
	V10SMb	I	80	352	1508	1591	81		
4	V5HWa	I	65	368	1758	1921	72	379	8.3%
	V5HWb	I	65	390	2040	2358	87		
5	V10HWa	II	80	315	1559	1623	62	386[(c)]	10.3%
	V10HWb	I	65	386	1810	2207	86		

Note: (a) All three strain gauges on the tension steel bars were damaged during the casting of concrete.
(b) The smallest of the mid-span deflections of the RC beams when the loading process was stopped was 27 mm (Specimen V0CBa);
(c) Only the beam which exhibited Crack pattern I is considered.

Table 10. Energy absorption of large-scale RC beam specimens

Batch	Specimen name	F_u (kN)	s_u (mm)	F_p (kN)	s_p (mm)	F_r (kN)	E_e (J)	E_{in} (J)	E_{total} (J)	Mean value of E_{total} (J)	Gain in the total energy absorbed due to FRP needles
1	V0CBa	366	8.38	44	15.38	55	1533.54	575.19	2108.73	2314.07	-
	V0CBb	333	7.20	75	8.40	67	1198.80	1320.60	2519.40		
2	V5SMa	315	6.44	120	7.66	84	1014.30	1972.68	2986.98	3082.86	33.2%
	V5SMb	248	4.98	153	5.92	90	617.52	2561.22	3178.74		
3	V10SMa	345	7.16	138	8.48	78	1235.10	2000.16	3235.26	3216.32	39.0%
	V10SMb	352	7.08	138	9.18	81	1246.08	1951.29	3197.37		
4	V5HWa	368	9.14	54	10.46	72	1681.76	1042.02	2723.78	3208.37	38.6%
	V5HWb	390	9.20	146	10.70	87	1794.00	1898.95	3692.95		
5	V10HWa	315	7.18	125	9.60	62	1130.85	1626.90	2757.75	3246.74	40.3%
	V10HWb	386	9.52	151	10.98	86	1837.36	1898.37	3735.73		

Note: F_u=ultimate load; s_u=deflection at F_u; F_p=load at post-peak plateau; s_p=deflection at the beginning of post-peak plateau; F_r=residual load when the mid-span deflection reached 27 mm; E_e=energy absorbed before the peak load, which was calculated as the area under the load-deflection curve from 0 to the peak load point; E_{in}=energy absorbed after the peak load, which was calculated as the area under the load-deflection curve from the peak load point to 27 mm; E_{total}=total energy absorbed, which was calculated as the area under the load-deflection curve from 0 to 27 mm.